Article

Chiral Inversion of Thiolate-Protected Gold Nanoclusters via Core Reconstruction without Breaking an Au-S Bond

Sami Malola, and Hannu Häkkinen

J. Am. Chem. Soc., **Just Accepted Manuscript** • DOI: 10.1021/jacs.9b01204 • Publication Date (Web): 19 Mar 2019

Chiral Inversion of Thiolate-Protected Gold Nanoclusters via Core Reconstruction without Breaking an Au-S Bond

Sami Malola and Hannu Häkkinen*

Departments of Physics and Chemistry, Nanoscience Center, University of Jyväskylä, FI-40014 Jyväskylä, Finland

Supporting Information Placeholder

ABSTRACT: Based on density functional theory computations of the well-known chiral $Au_{38}(SR)_{24}$ nanocluster and its Pd- and Ag-doped derivatives, we propose here a mechanism for chiral inversion that does not require breaking of a metal-sulfur bond at the metal-ligand interface, but features a collective rotation of the gold core. The calculated energy barriers for this mechanism for Au_{38} and Pd-doped Au_{38} are in the range of 1 – 1.5 eV, significantly lower than barriers involving breakage of Au-S bonds (2.5 eV). For Ag-doped Au_{38}, barriers for both mechanisms are similar (1.3 – 1.5 eV). Inversion barriers for a larger chiral $Au_{144}(SR)_{60}$ are much higher (2.8 eV). Our computed barriers are in a good agreement with racemization barriers estimated from existing experiments for bare and doped Au_{38}. These results highlight the sensitivity of chiral inversion to the size, structure and metal composition of the metal core and sensitivity to the detailed structure of the metal-thiolate interface. Our work also predicts that enantiopure $Au_{144}(SR)_{60}$ clusters would be promising materials for applications requiring high resistance to chiral inversion.

Introduction

Chirality is instrumental to many functions and processes of biomolecules, surface reactions, and organic catalysis, to name a few. In recent years, several structurally characterized metal nanoclusters protected by organic surface ligands (the so-called monolayer protected clusters, MPCs) are found chiral at various levels due to the metal core, ligand layer or metal-ligand interface structures.[1-3] The first structurally resolved members of gold-based MPCs emerged in 2007 after which the research filed has been rapidly growing.[1,4,5]

The unique intrinsic chirality of molecules and nanoclusters is a basis for many interesting applications of sensing and catalysis utilizing the rich chiroptical properties. Challenges are usually related to achieving good enantioselectivity and resistance to racemization at elevated temperatures. Experimental work on chiral MPCs has successfully surveyed separation of chiral enantiomers during and after synthesis,[6-10] properties affecting chiral activity as well as thermal stability against chiral inversion.[6,11-16] One of the most extensively studied clusters in this perspective is the prolate, bi-icosahedral $Au_{38}(SR)_{24}$ and its derivatives afforded by doping or ligand-exchange. For this cluster, relatively low activation barriers (0.8-1.3 eV) have been reported experimentally for the racemization which doping and ligand-exchange affects.[11-14] Surprisingly, the reported barriers are way too low for reactions including breaking Au-S bonds on the cluster surface[1b] which would be the most obvious way to rearrange the Au-S interface structure into an opposite chirality.

Two possible mechanisms for the chiral inversion of $Au_{38}(SR)_{24}$ have been introduced previously: (i) SN2-type of mechanism for protecting unit rearrangement and (ii) S-atom "sliding" mechanism.[11] Both of the mechanisms require simultaneous Au-S bond breaking and formation. Despite of the proposed mechanisms, the experimental observations have remained unexplained. In contradiction to $Au_{38}(SR)_{24}$, there are examples of other MPCs that are much more stable against racemization under heating which raises unanswered questions about the uniqueness of racemization mechanism with respect to the specific cluster type.[6]

In this work, we have computationally investigated detailed mechanisms and energy barriers for MPC racemization concentrating first on $Au_{38}(SR)_{24}$ and its doped derivatives. The findings

about the plausible racemization mechanisms are generalized for another larger, well-known, chiral MPC, $Au_{144}(SR)_{60}$. With the proposed mechanisms we can explain experimental observations of racemization in detail and show that the racemization of MPCs is indeed unique for each individual cluster depending critically on the specific structure of the metal-ligand interface and especially on the structure of the metal core. These results will deepen the knowledge about stability of MPCs against different structural reconstructions which can be crucial for explaining, for instance, metal atom exchange in cluster-cluster interactions or structural reconstructions during ligand-exchange.[17-26] Our main result is that metal-sulfur bond breaking is not needed for the full racemization of $Au_{38}(SR)_{24}$, not even as an associative SN2 type of process in which metal-sulfur bonds break and form simultaneously. The low-energy mechanism of $Au_{38}(SR)_{24}$ racemization includes only a reconstruction of the metal core, for which the activation barrier is much lower than for the studied Au-S bond breaking reactions. Additionally, we show that in the small icosahedral MPCs $Au_{25}(SR)_{18}$ this kind of reconstruction may exist with comparably low activation energies leading to isomer structures different from the known measured structures. These rather low-energy isomers exhibit a more sterically open ligand shell allowing possible cluster – cluster interactions.

Computational Method

We used the numerical implementation of the density functional theory (DFT) in code-package GPAW.[27] Real-space grid with 0.2 Å grid spacing, PBE xc-functional[28] and 0.05 eV/Å criterion for the residual forces on atoms was used for the structural relaxation. The initial structures of $Au_{38}(SR)_{24}$, $Pd_2Au_{36}(SR)_{24}$, $Ag_9Au_{29}(SR)_{24}$, and $Au_{25}(SR)_{18}^-$ clusters were based on the experimentally reported structures and their most probable Pd/Ag doping sites.[29-30] The initial structure for the $Au_{144}(SR)_{60}$ was based on the theoretical prediction by Lopez-Acevedo et al.[31], which was very recently shown to be the correct one by the single-crystal X-ray structure of Jin and Wu groups.[32] Methylthiolate (SCH_3) was used as a simple model ligand to reduce the computational cost for Au_{25}, Au_{38}, Pd_2Au_{36}, and Ag_9Au_{29}, and SH was used as the ligand for Au_{144}. Atomic visualizations of the starting structures of Au_{25}, Au_{38} and Au_{144} clusters are shown in Figure 1.

Two mechanisms of chiral inversion were investigated using constrained structural relaxation (see schematics in Figure S1). In the first mechanism, a number of core metal atoms were selected for rotational transformation applied around the principal symmetry axis (3 atoms around C3 for Au_{38} and its derivatives as well as for Au_{25} and 5 atoms around C5 for Au_{144}). The rotations were done in steps of 5-6 degrees. In the second mechanism, sliding transformations of S-atoms were applied linearly between the initial and final binding sites in 0.2 Å steps by keeping the minimum metal-sulfur distance equal to the initial bond distances. A constraint of fixing two atomic distances was applied for the atoms responsible of the transformations. In the case of rotational transformation, distances to two other metal core atoms were fixed for each active metal atom. For the S-atom sliding transformations, distances to the initial and final metal atom binding positions were fixed for each active sulfur atom. Both of the mentioned constraints were obligatory in order to drive the system over the transition state. Further constrained relaxations were done (if necessary) starting from the optimized structures of the first constrained relaxation in order to increase the accuracy of the calculated energy barriers. For these follow up relaxations, done for Au_{38} and its derivatives, three metal atoms in the both ends of the 23 atom metal core were fixed, but the rest of the atoms were free. The selected approach ensures that the non-relevant strain accumulated into the structure gets released. In total for all systems, about 700 relaxations to a local energy minimum were performed.

Results and Discussion

Au_{38} and its derivatives. We first investigated two different mechanisms for the racemization of $Au_{38}(SR)_{24}$, $Pd_2Au_{36}(SR)_{24}$ and $Ag_9Au_{29}(SR)_{24}$ clusters: S-atom sliding between two adjacent Au-atom binding sites and rotational transformation of selected metal atoms of the core. The first mechanism requires simultaneous Au-S bond breaking and formation whereas the second is about reconstruction the metal core without Au-S bond breaking. In both cases the rearrangement of the three long protecting units into the opposite chirality around the principal symmetry axis follows from the driven structural changes. Transformations were conducted simultaneously for all the selected active atoms, and for one end of the bi-icosahedral cluster in time. In general, transformation at one end is enough for estimating reliably the activation energy for the whole mechanism as it leads to an intermediate structure that is symmetric between the left and the right-handed enantiomers. The complete chirality inversion was modeled only for the Au38(SR)24 cluster.

As a starting point we modeled the previously suggested mechanism of S-atom sliding between their adjacent binding sites around the principal symmetry axis.[11] The rate determining step of that mechanism is the jump of S-atoms between their binding sites, which must be conducted twice in the both icosahedral ends for the full chiral inversion process. Hence, to estimate if the suggested mechanism can provide explanation to the experimentally measured results, the first jump of S-atom sliding was modeled for each of the studied clusters $Au_{38}(SR)_{24}$, $Pd_2Au_{36}(SR)_{24}$ and $Ag_9Au_{29}(SR)_{24}$. During the mechanism, metal core atoms' rotation gets slightly correlated with the S-atom sliding, but the exchange between the binding sites remains as a rate determining step defining the transition state. This is confirmed by the energy behavior as a function of the relaxation step and the relaxed structures of the selected frames that are shown in Figure 2 (see also an animation of the mechanism in SI video "Au38_Satom_sliding.avi").

Calculated energy barriers for the S-atom sliding were 2.5 eV for $Au_{38}(SR)_{24}$ and $Pd_2Au_{36}(SR)_{24}$ clusters but only 1.55 eV for $Ag_9Au_{29}(SR)_{24}$ cluster. The barrier of $Au_{38}(SR)_{24}$ and $Pd_2Au_{36}(SR)_{24}$ clusters is in agreement with the strength of the Au-S bond. Flexibility of Ag-atoms binding properties with thiolates compared to Au-atoms explains the difference to the Ag-doped cluster. For example, metal-sulfur coordination of the silver atoms on known MPCs can vary between 2 and 4 as it is 2 for the surface Au-atoms. The energy barriers of sliding mechanism of $Au_{38}(SR)_{24}$ and $Pd_2Au_{36}(SR)_{24}$ clusters are 1.2 eV and 1.6 eV higher, respectively, compared to experimentally measured results of 1.3 eV and 0.9 eV.[11,14] Therefore S-atom sliding can possibly exist only during chiral inversion of the measured $Ag_xAu_{38-x}(SR)_{24}$ clusters, for which the experimentally measured activation energy is 0.9 eV.[13] It is of interest to remark that one of the high energy conformations at 2.5 eV shows detachment of one of the core gold atoms out from core surface as is visualized for $Pd_2Au_{36}(SR)_{24}$ cluster in frame 13 of Figure 2(b),(e). This observation indicates that also other more complex mechanism affecting the conformation of the protecting units by simultaneous Au-S bond breaking and formation can be excluded.

Because of the discrepancy between the calculated and experimental results we proceeded to study other possible mechanisms. Metal clusters may transform by rearrangements of atomic layers or changing the packing of atoms. These transformations may include for example sliding of atomic layers with respect to each other. In the case of $Au_{38}(SR)_{24}$ cluster and its doped derivatives, there exists a simple metal core transformation mechanism that leads to the full chiral inversion. By rotating the three outermost Au-atoms of the metal core close to both of the poles of the principal C3 symmetry axis of the cluster, the protecting units can be rearranged automatically into the opposite handedness without any Au-S bond breaking. Thus, reconstruction of the metal core is solely responsible for the inversion.

The results for the rotational transformation mechanism of the Au-core are shown in Figure 3 for $Au_{38}(SR)_{24}$, $Pd_2Au_{36}(SR)_{24}$ and $Ag_9Au_{29}(SR)_{24}$ clusters (see also animations in SI videos "Au38_core_reconstruction.avi", "Pd2Au36_core_reconstruction.avi", and "Ag9Au29_core_reconstruction.avi"). The full chiral inversion is modeled for $Au_{38}(SR)_{24}$ cluster whereas only the first half of the process is modeled for $Pd_2Au_{36}(SR)_{24}$ and $Ag_9Au_{29}(SR)_{24}$ clusters. Remarkably, the energy barriers for both $Au_{38}(SR)_{24}$ and $Pd_2Au_{36}(SR)_{24}$ drop below 1.5 eV as compared to barriers of the S-atom sliding mechanism. Considering the fluctuations in energy close to the top of the barriers, the calculated barrier heights lie in the range of 1.3 – 1.5 eV for $Au_{38}(SR)_{24}$, 1.0 – 1.4 eV for $Pd_2Au_{36}(SR)_{24}$ and 1.1 – 1.3 eV for $Ag_9Au_{29}(SR)_{24}$ cluster.

Detailed structural analysis of the rotational transformation mechanism reveals that the active end of the metal core transforms first from the icosahedral symmetry more into FCC- or HCP-packed atomic layers resembling cubo-octahedral symmetry, after which it transforms back to the icosahedral symmetry when approaching the achiral intermediate conformation. The cubo-octahedral arrangement is seen as a local minimum energy structure along the reaction path as is pointed out for example in the frame 31 of Figure 3a) (see also the corresponding part of the SI video file "Au38_core_reconstruction.avi"). The $Au_2(SR)_3$ protecting units get protruded out from the core surface during the transformation, which is also observed in the intermediate local minimum energy structure.

The general observation based on the calculated results is that doping of the cluster with Pd- or Ag-atoms decreases the energy barrier of reconstructing the metal core. The result is contrary to the previous assumptions that the doping increases the stability of the cluster especially regarding the metal core. However, our finding is in a very good agreement with the experimentally measured results on racemization, which were thought to be explained by the decreased strength of Au-S bonds.[11-14] Experimentally measured activation energies for Pd- and Ag-doped clusters, $Pd_2Au_{36}(SR)_{24}$ and $Ag_xAu_{38-x}(SR)_{24}$, are reported to be around 0.9 eV with no major differences between the two systems

whereas for $Au_{38}(SR)_{24}$ cluster the barrier is close to 1.3 eV. [11-14] A similar trend can be seen in the calculated results despite of the minor systematic overestimation in the energy barriers. After all, the reconstruction of the metal core by rotational transformation is perfectly explaining the experimental observation of rather low activation energies and effects on that by doping. Our interpretation is that the energy landscape for isomerization of the metal core is more shallow for the doped clusters than for the pure gold MPCs. Our results indicate that the metal core reconstruction is mainly responsible for the racemization in all of the studied systems. For $Ag_9Au_{29}(SR)_{24}$ cluster S-atom sliding type of SN2 mechanisms may be also important which could explain the measured differences in the reaction entropy between $Ag_xAu_{38-x}(SR)_{24}$ and $Au_{38}(SR)_{24}$ clusters.

Chiral inversion of Au_{144}. The studied rotational reconstruction mechanism of the metal core can be generalized also to other chiral MPCs. For example, $Au_{144}(SR)_{60}$ cluster was first predicted,[31] and recently confirmed,[32] to be chiral because of the binding and overall conformation of the short protecting RS-Au-SR units on the surface. The outermost anti-Mackay atomic layer of the three-layer icosahedral metal core and the highly symmetric Au-S interface allow a similar type of rotational transformation of the metal core as in $Au_{38}(SR)_{24}$. By rotating the five Au-atoms of the outermost core layer, closest to each of the C5 symmetry axis, the chirality of the cluster gets inversed without any Au-S bond breaking. The results of rotational transformation of the first five atoms around one of the C5 axis are shown in Figure 4 (see also the animation in SI video "Au144_core_reconstruction.avi"). The energy barrier for the mechanism is 2.8 eV which is slightly larger than the Au-S bond strength and the energy barrier of the S-atom sliding mechanism in $Au_{38}(SR)_{24}$ but much higher than the barrier of metal core transformation in $Au_{38}(SR)_{24}$. These results indicate that $Au_{144}(SR)_{60}$ is much more stable against racemization as compared to $Au_{38}(SR)_{24}$ or its doped derivatives. It also suggests that the S-atom sliding mechanism may be relevant for chiral inversion of the larger clusters. This implies that the racemization mechanism and stability strongly depend on the size, core structure, and the details of the metal-ligand interface.

Core reconstruction of Au_{25}. Finally, we broadened the idea about the metal core transformation to one more MPC, $Au_{25}(SR)_{18}^-$, that has also an icosahedral core but consists only of one Au13 icosahedron instead of the face-fuced bi-icosahedron of $Au_{38}(SR)_{24}$. The arrangement of the protecting units is partly analogous to the arrangement of $Au_{38}(SR)_{24}$ cluster and the same rotational reconstruction mechanism can be applied on one side of the Au-core as in $Au_{38}(SR)_{24}$ (see the animation in SI video "Au25_core_reconstruction.avi"). The calculated energy barrier of 1.30 eV for $Au_{25}(SR)_{18}$ is in line with the results for $Au_{38}(SR)_{24}$ as is shown in Figure 5. This indicates that for small icosahedral MPCs, the energy barrier for the Au-core reconstruction are of the same order, in general considerably low.

$Au_{25}(SR)_{18}$- is not chiral, so the calculated energy barrier is not relevant for racemization. However, it is very interesting to note that a new local energy minimum configuration is found only 0.70 eV higher in energy as a consequence of the studied rotational reconstruction with rather low formation barrier (frame 42 in Figure 5). Compared to the initial structure, this intermediate configuration has a more open surface structure due to three protruded long protecting units. We believe that this kind of isomeric structures could provide new insights for explaining also other previously reported low energy reactions and processes between MPCs like the metal atom exchange which is expected to happen between the core metal atoms of two different clusters.[17-22] Hence, in the same experimental conditions that racemizes $Au_{38}(SR)_{24}$ cluster, also $Au_{25}(SR)_{18}^-$ cluster should be easily reconstructed by its core. These small icosahedral MPCs may be more prone to cluster-cluster interactions and atomic exchange exactly due these special low energy metal core reconstructions that can spatially reveal part of the surface. Interestingly, also the reports on these experiments have heavily concentrated on small icosahedral clusters like $Au_{25}(SR)_{18}$ and $Au_{38}(SR)_{24}$ or their Ag-atom doped derivatives, or protected silver clusters. In general, pure silver and silver doped MPCs are more vulnerable for reconstructions due to the flexibility of Ag-S coordination as the results of this study already showed. Therefore, selecting small icosahedral gold MPCs for a counterpart in cluster-cluster reactions may be the most important key behind the results again because of low energy metal core reconstructions. Our results here rationalize further why many MPCs undergo easily also metal core reconstructions during ligand-exchange experiments as the energy barriers for the metal core reconstructions are of the same order or even remarkably lower compared to the reactions of Au-S bond breaking.[24-26]

Conclusions

We have studied computationally possible mechanisms for chiral inversion of $Au_{38}(SR)_{24}$ cluster and its Pd- and Ag-atom doped derivatives.

The results show that the chiral inversion of the cluster can happen energy-optimally without any Au-S bond breaking through a rotational reconstruction of the metal core. Furthermore, doping of the cluster core with Pd- or Ag-atoms decreases the energy barrier for the inversion. All the calculated results match very well with the previously reported experimental results and rationalize the observations for which no explanation has been given before. The suggested metal core transformation can be generalized also for other monolayer protected metal clusters such as $Au_{144}(SR)_{60}$ and $Au_{25}(SR)_{18}$-. In general, it is known from experiments on gold-MPCs that gold-gold vibrational modes are softer than gold-sulfur modes at the metal-ligand interface,[35] and we expect the collective soft core rotational modes to induce the suggested core reconstructions leading to chiral inversion. In general, the interactions in the ligand layer between the ligand molecules are distinctly weaker which leads to a very dynamic layer even at room temperature (see, *e.g.*, Fig. 3 and an accompanying animation video of the simulated ligand dynamics of pMBA ligands in $Au_{102}(pMBA)_{44}$ in ref. 36, and an early DFT molecular dynamics study of $Au_{25}(SH)_{18}^-$ in ref. 37 about the gold-ligand interface dynamics). These weaker interactions can thus be expected to adjust to core transformations, except for special cases such as when bi-dentate ligands are used to stabilize the ligand layer.[12]

Our work suggests that the stability against chiral inversion is a unique property of each individual MPC depending on the metal-ligand interface and especially metal core structure. These results are believed to be important for development of sustainable applications using the intriguing chiroptical properties of MPCs by a better understanding of the effects of chiral stability. Our work also implies that in case that enantiopure samples of $Au_{144}(SR)_{60}$ clusters could be made, those materials would resist chiral inversion at elevated temperatures. This is particularly interesting in light of the recent calculation showing a very strong chiral dichroism (CD) signal from one of the enantiomers of $Au_{144}(SR)_{60}$.[38] Furthermore, these results may provide new insights for explaining other interesting observations on MPCs such as cluster-cluster interactions, metal atom exchange and cluster transformations, also seen at rather low temperatures.

ASSOCIATED CONTENT

Supporting Information

Figure S1 showing schematics of S-atom sliding and core rotation mechanism for chiral inversion. Six videos (.avi format) showing animations of the mechanisms for $Au_{38}(SCH_3)_{24}$, $Pd_2Au_{36}(SCH_3)_{24}$, $Ag_9Au_{29}(SCH_3)_{24}$, $Ag_{25}(SCH_3)_{18}^-$, and $Au_{144}(SH)_{60}$. This material is available free of charge via the Internet at http://pubs.acs.org.

AUTHOR INFORMATION

Corresponding Author

hannu.j.hakkinen@jyu.fi

ORCID

Hannu Häkkinen: 0000-0002-8558-5436

Notes

The authors declare no competing financial interests.

ACKNOWLEDGMENT

We acknowledge funding from the Academy of Finland (projects 294217 and 315549 and HH's Academy Professorship) as well as generous CPU resources from the CSC supercomputer center in Espoo, Finland, and from the Barcelona Supercomputing Center, Spain, in the PRACE project NANOMETALS.

REFERENCES

(1) (a) Tsukuda, T.; Häkkinen, H. *Protected Metal Clusters: From Fundamentals to Applications*, Elsevier, Amsterdam **2015**; (b) Häkkinen, H. The Gold-Sulfur Interface at the Nanoscale. *Nature Chem.* **2012**, *4*, 443-455; (c) Fernando, A.; Weerawardene K.L.D.M.; Karimova, N.V.; Aikens, C.M. Quantum Mechanical Studies of Large Metal, Metal Oxide, and Metal Chalcogenide Nanoparticles and Clusters, *Chem. Rev.* **2015**, *115*, 6112-6216.

(2) (a) Gautier, C.; Burgi, T. Chiral Gold Nanoparticles, *ChemPhysChem* **2009**, 10, 483-492; (b) Knoppe, S.; Burgi, T. Chirality in Thiolate-Protected Gold Clusters. *Acc. Chem. Res.* **2014**, *47*, 1318-1326.

(3) Knoppe, S. Chirality in Ligand-Stabilized Metal Clusters, In *Encyclopedia of Interfacial Chemistry*, Elsevier, Oxford, **2018**, 406-416.

(4) Jadzinsky, P.D.; Calero, G.; Ackerson, C.J.; Bushnell D.A.; Kornberg, R.D. Structure of a Thiol Monolayer-Protected Gold Nanoparticle at 1.1 Angstrom Resolution, *Science* **2007**, *318*, 430–433.

(5) Walter, M.; Akola, J.; Lopez-Acevedo, O.; Jadzinsky, P.D.; Calero, G.; Ackerson, C.J.; Whetten, R.L.; Grönbeck, H.; and Häkkinen, H. A Unified View of Ligand-Protected Gold Clusters as Superatom Complexes, *Proc. Natl. Acad. Sci. USA* **2008**, *105*, 9157–9162.

(6) Deng, G.; Malola, S.; Yan, J.; Han, Y.; Yuan, P.; Zhao, C.; Yuan, X.; Lin, S.; Tang, Z.; Teo, B.K.; Häkkinen, H.; Zheng N. From Symmetry Breaking to Unraveling the Origin of the Chirality of Ligated Au13Cu2 Nanoclusters, *Angew. Chem. Int. Ed.* **2018**, *57*, 3421.

(7) Yan, J.; Su, H.; Yang, H.; Hu, C.; Malola, S.; Lin, S.; Teo, B.K.; Häkkinen, H.; Zheng, N. Asymmetric Synthesis of Chiral Bimetallic [Ag28Cu12(SR)24]4– Nanoclusters via Ion Pairing, *J. Am. Chem. Soc.*, **2016**, *138*, 12751–12754.

(8) Knoppe, S.; Wong, O.A.; Malola, S.; Häkkinen, H.; Bürgi, T.; Verbiest, T.; Ackerson, C.J. Chiral Phase Transfer and

Enantioenrichment of Thiolate-Protected Au102 Clusters, *J. Am. Chem. Soc.* **2014,** *136*, 4129-4132.

(9) Dolamic, I.; Knoppe, S.; Dass, A.; Burgi, T. First Enantioseparation and Circular Dichroism Spectra of Au38 Clusters Protected by Achiral Ligands, *Nature Comm.* **2012**, *3*, 798.

(10) Yang, H.; Yan, J.; Wang, Y.; Deng, G.; Su, H.; Zhao, X.; Xu, C.; Teo, B.K.; Zheng, N. From Racemic Metal Nanoparticles to Optically Pure Enantiomers in One Pot, *J. Am. Chem. Soc.* **2017,** *139*, 16113-16116.

(11) Knoppe, S.; Dolamic, I.; Burgi, T. Racemization of a Chiral Nanoparticle Evidences the Flexibility of the Gold-Thiolate Interface, *J. Am. Chem. Soc.* **2012,** *134*, 13114-13120.

(12) Knoppe, S.; Michalet, S.; Burgi, T. Stabilization of Thiolate-Protected Gold Clusters Against Thermal Inversion: Diastereomeric $Au_{38}(SCH_2CH_2Ph)_{24-2X}(R\text{-}BINAS)_X$, *J. Phys. Chem. C* **2013**, *117*, 15354-15361.

(13) Zhang B.; Burgi, T. Doping Silver Increases the Au38(SR)24 Cluster Surface Flexibility, *J. Phys. Chem. C* **2016**, *120*, 4660-4666.

(14) Barrabes, N.; Zhang B.; Burgi, T. Racemization of Chiral $Pd_2Au_{36}(SCH_2CH_2Ph)_{24}$: Doping Increases the Flexibility of the Cluster Surface, *J. Am. Chem. Soc.* **2014**, *136*, 14361-14364.

(15) Knoppe, S.; Dolamic, I.; Dass, A.; Bürgi, T., Separation of Enantiomers and CD Spectra of $Au_{40}(SCH_2CH_2Ph)_{24}$: Spectroscopic Evidence for Intrinsic Chirality. *Angew. Chem. Int. Ed.* **2012**, *51*, 7589-7591.

(16) Malola, S.; Lehtovaara, L.; Knoppe, S.; Hu, K-J.; Palmer, R.E.; Bürgi, T.; Häkkinen, H. Au-40(SR)(24) Cluster as a Chiral Dimer of 8-Electron Superatoms: Structure and Optical Properties, J. *Am. Chem. Soc.* **2012,** *134*, 19560-19563.

(17) Krishnadas, K.R.; Baksi, A.; Ghosh, A.; Natarajan G.; Pradeep, T. Structure-Conserving Spontaneous Transformations Between Nanoparticles, *Nature Comm.* **2016**, *7*, 13447.

(18) Krishnadas, K.R.; Baksi, A.; Ghosh, A.; Natarajan, G.; Som, A.; Pradeep, T. Interparticle Reactions: An Emerging Direction in Nanomaterials Chemistry, *Acc. Chem. Res.* **2017,** *50*, 1988-1996.

(19) Krishnadas, K.R.; Ghosh, A.; Baksi, A.; Chakraborty, I.; Natarajan, G.; Pradeep, T. Intercluster Reactions Between Au25(SR)18 and Ag44(SR)30, *J. Am. Chem. Soc.* **2016,** *138*, 140-148.

(20) Krishnadas, K.R.; Ghosh, D.; Ghosh, A.; Natarajan, G.; Pradeep, T. Structure–Reactivity Correlations in Metal Atom Substitutions of Monolayer-Protected Noble Metal Alloy Clusters, *J. Phys. Chem. C* **2017,** *121*, 23224-23232.

(21) Zhang, B.; Safonova, O.V.; Pollitt, S.; Salassa, G.; Sels, A.; Kazan, R.; Wang, Y.; Rupprechter, G.; Barrabés, N; Bürgi, T. On the Mechanism of Rapid Metal Exchange Between Thiolate-Protected Gold and Gold/Silver Clusters: A Time-Resolved in situ XAFS study, *Phys. Chem. Chem. Phys.*, **2018,** *20*, 5312-5318.

(22) Zhang, B.; Salassa, G.; Bürgi, T. Silver Migration Between Au38(SC2H4Ph)24 and doped AgxAu38–x(SC2H4Ph)24 Nanoclusters, *Chem. Commun.* **2016,** *52*, 9205-9207.

(23) Salassa, G.; Sels, A.; Mancin, F.; Bürgi, T. Dynamic Nature of Thiolate Monolayer in Au25(SR)18 Nanoclusters, *ACS Nano* **2017,** *11*, 12609-12614.

(24) Zeng, C.; Liu, C.; Pei, Y.; Jin, R. Thiol Ligand-Induced Transformation of Au38(SC2H4Ph)24 to Au36(SPh-t-Bu)24, *ACS Nano* **2013,** *7*, 6138-6145.

(25) Nimmala, P.R.; Theivendran, S.; Barcaro, G.; Sementa, L.; Kumara, C.; Jupally, V.R.; Apra, E.; Stener, M.; Fortunelli, A.; Dass, A. Transformation of Au144(SCH2CH2Ph)60 to Au133(SPh-tBu)52 Nanomolecules: Theoretical and Experimental Study, *J. Phys. Chem. Lett.* **2015,** *6*, 2134-2139.

(26) Dass, A.; Theivendran, S.; Nimmala, P.R.; Kumara, C.; Jupally, V.R.; Fortunelli, A.; Sementa, L.; Barcaro, G.; Zuo, X.; Noll, G. Au133(SPh-tBu)52 Nanomolecules: X-ray Crystallography, Optical, Electrochemical, and Theoretical Analysis, *J. Am. Chem. Soc.* **2015,** *137*, 4610-4613.

(27) Enkovaara, J.; Rostgaard, C.; Mortensen, J.J.; Chen, J.; Dulak, M.; Ferrighi, L.; Gavnholt, J.; Glinsvad, C.; Haikola, V.; Hansen, H.A.; Kristoffersen, H.H.; Kuisma, M.; Larsen, A.H.; Lehtovaara, L.; Ljungberg, M.; Lopez-Acevedo, O.; Moses, P.G.; Ojanen, J.; Olsen, T.; Petzold, V.; Romero, N.A.; Stausholm, J.; Strange, M.; Tritsaris, G.A.; Vanin, M.; Walter, M.; Hammer, B.; Häkkinen, H.; Madsen, G.K.H.; Nieminen, R.M.; Norskov, J.K.; Puska, M.; Rantala, T.T.; Schiotz, J.; Thygesen, K.S.; Jacobsen, K.W. Electronic Structure Calculations with GPAW: A Real-Space Implementation of the Projector Augmented-Wave Method *J. Phys. Condens. Matter* **2010,** 22, 253202.

(28) Perdew, J.P.; Burke, K.; Ernzerhof, M. Generalized Gradient Approximation Made Simple, *Phys. Rev. Lett.* **1996**, 77, 3865-3868.

(29) (a) Qian, H.; Eckenhoff, W.T.; Zhu, Y.; Pintauer, T.; Jin, R. Total Structure Determination of Thiolate-Protected Au38 Nanoparticles, *J. Am. Chem. Soc.* **2010,** *132*, 8280-8281; (b) Zhang, B.; Kaziz, S.; Li, H.; Wodka, D.; Malola, M.; Safonova, O.; Nachtegaal, M.; Mazet, C.; Dolamic, I.; Llorca, J.; Kalenius, E.; Daku, L.M.L.; Häkkinen, H.; Bürgi, T.; Barrabés, N. Pd2Au36(SR)24 Cluster: Structure Studies, *Nanoscale*, **2015**, *7*, 17012-17019; (c) Kumara, C.; Gagnon, K.J.; Dass, A. X-ray Crystal Structure of Au38–xAgx(SCH2CH2Ph)24 Alloy Nanomolecules, *J. Phys. Chem. Lett.* **2015**, *6*, 1223-1228.

(30) (a) Heaven, M.W, Dass, A.; White, P.S.; Holt, K.M.; Murray, R.W. Crystal Structure of the Gold Nanoparticle [N(C8H17)4][Au25(SCH2CH2Ph)18]. *J. Am. Chem. Soc.* **2008**, *130*, 3754-3755; (b) Zhu, M.; Aikens, C.M.; Hollander, F.J.; Schatz, G.C.; Jin, R. Correlating the Crystal Structure of A Thiol-Protected Au25 Cluster and Optical Properties. *J. Am. Chem. Soc.* **2008**, *130*, 5883-5885.

(31) Lopez-Acevedo, O.; Akola, J.; Whetten, R.L.; Grönbeck, H.; Häkkinen, H. Structure and Bonding in the Ubiquitous Icosahedral Metallic Gold Cluster Au144(SR)60. *J. Phys. Chem. C.* **2009**, *113*, 5035-5038.

(32) Yan, N.; Xia, X.; Liao, L.; Zhu, M.; Jin, M.; Jin, R.; Wu, Z. Unravelling the Long-Pursued Au144 Structure by X-ray Crystallography, *Sci. Adv.* **2018**, *4*, eaat7259.

(35) Yamazoe, S.; Takano, S.; Kurashige, W.; Yokoyama, T.; Nitta, K. Negishi, Y.; Tsukuda, T. Hierarchy of Bond Stiffnesses within Icosahedral-Based Gold Clusters Protected by Thiolates. *Nature Comm.* **2016**, *7*, 10414-10414.

(36) Salorinne, K.; Malola, S.; Wong, O.A.; Rithner, C.D.; Chen, X.; Ackerson, C.J.; Häkkinen, H. Conformation and Dynamics of the Ligand Shell of a Water-Soluble Au102 Nanoparticle. *Nature Comm.* **2016**, *7*, 10401.

(37) Mäkinen, V.; Häkkinen, H. Density Functional Theory Molecular Dynamics Study of the $Au_{25}(SH)_{18}^-$ Cluster. *Eur. Phys. J D* **2012**, *66*, 310.

(38) Malola, S.; Kaappa, S.; Häkkinen, H. From Molecular to Metallic Gold Nanoparticles: The Role of Nanocrystal Symmetry in the Crossover Region. Preprint (2018) at: https://arxiv.org/abs/1809.04411

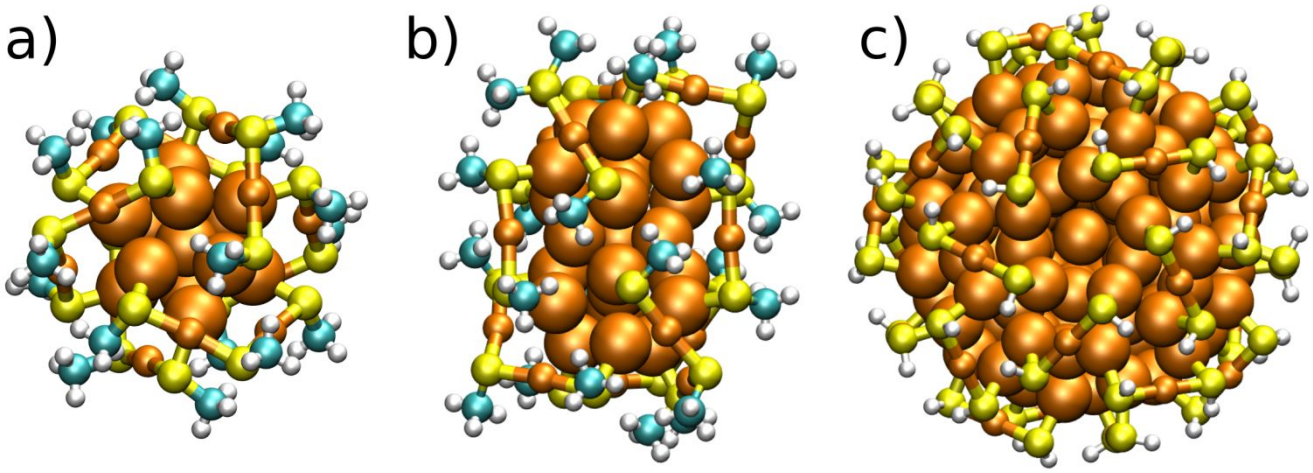

Figure 1. Atomic structures of the computational models for (a) $Au_{25}(SCH_3)_{18}^-$; (b) $Au_{38}(SCH_3)_{24}$; and (c) $Au_{144}(SH)_{60}$. The structures in (a) and (b) are based on the respective experimental crystal structures (refs. 30 and 29a). The structure in (c) is from ref. 31. Colors: H (white), C (cyan), S (yellow), Au (orange).

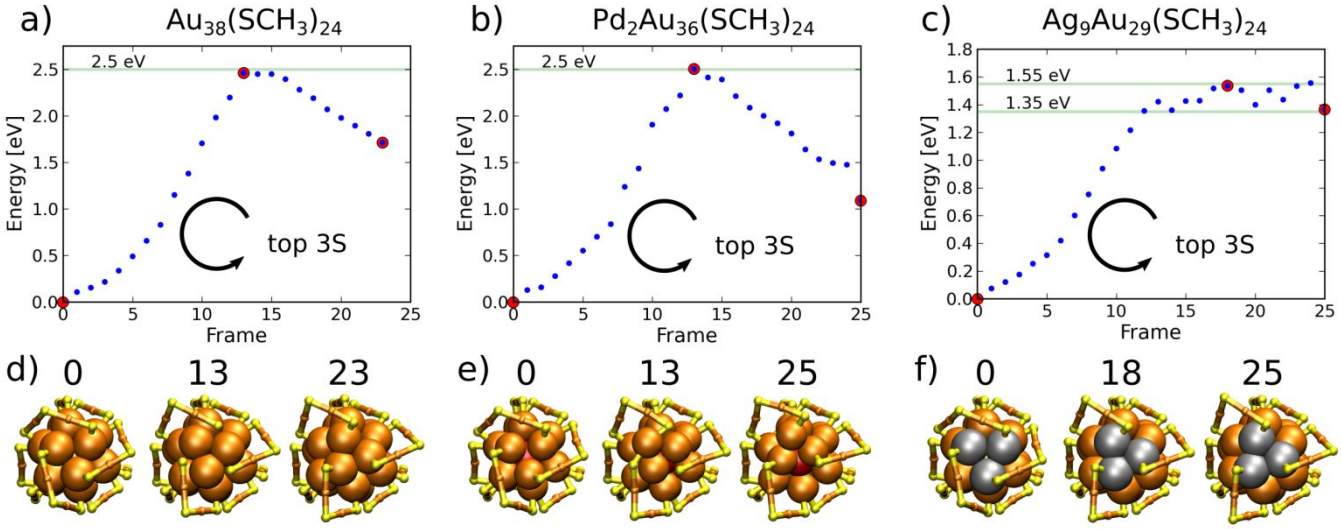

Figure 2. Inversion energy profiles and selected configurations of (a), (d): $Au_{38}(SCH_3)_{24}$, (b),(e): $Pd_2Au_{36}(SCH_3)_{24}$ and (c),(f): $Ag_9Au_{29}(SCH_3)_{24}$ clusters by sliding of three S-atoms to their neighboring binding site. Three selected snapshots (frames) labeled by red dots in (a)-(c) are visualized below each panel. Only the gold-sulfur framework is shown for clarity. Arrows denote the direction for sliding of the three S-atoms of the outermost core layer closest to the principal symmetry axis C_3 at both ends. Au: orange, S: yellow, Ag: gray, Pd: red.

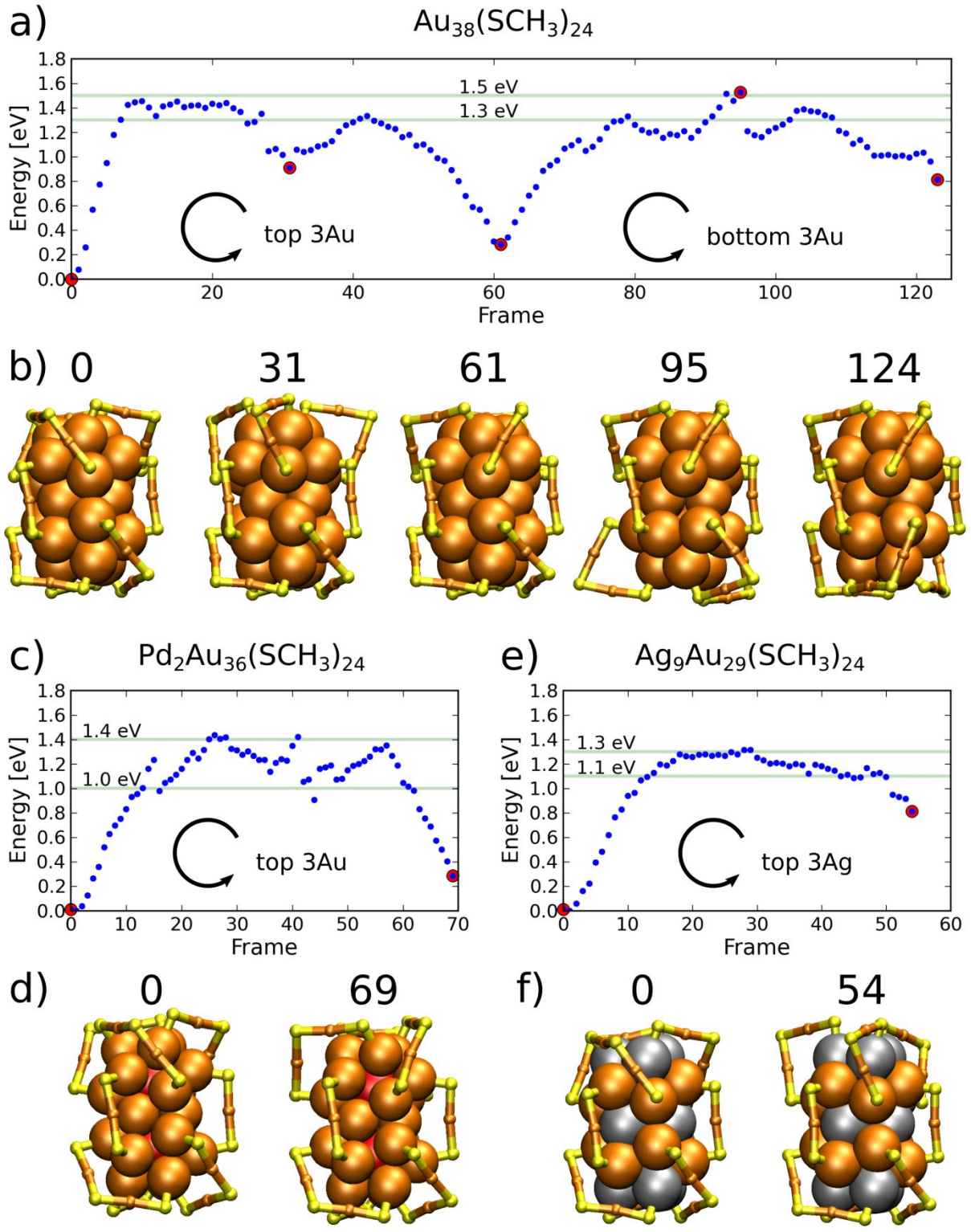

Figure 3. Inversion energy profiles and selected configurations of (a), (b) $Au_{38}(SCH_3)_{24}$, (c), (d) $Pd_2Au_{36}(SCH_3)_{24}$ and (e), (f) $Ag_9Au_{29}(SCH_3)_{24}$ clusters by rotation of core Au- and Ag-atoms. Selected configurations labeled by red dots in the energy curves are visualized below each panel. Only the metal-sulfur framework is shown for clarity. Arrows denote the direction of the rotation of three Au- or Ag-atoms closest to the principal symmetry axis at both ends of the cluster core. Colors as in Fig 2.

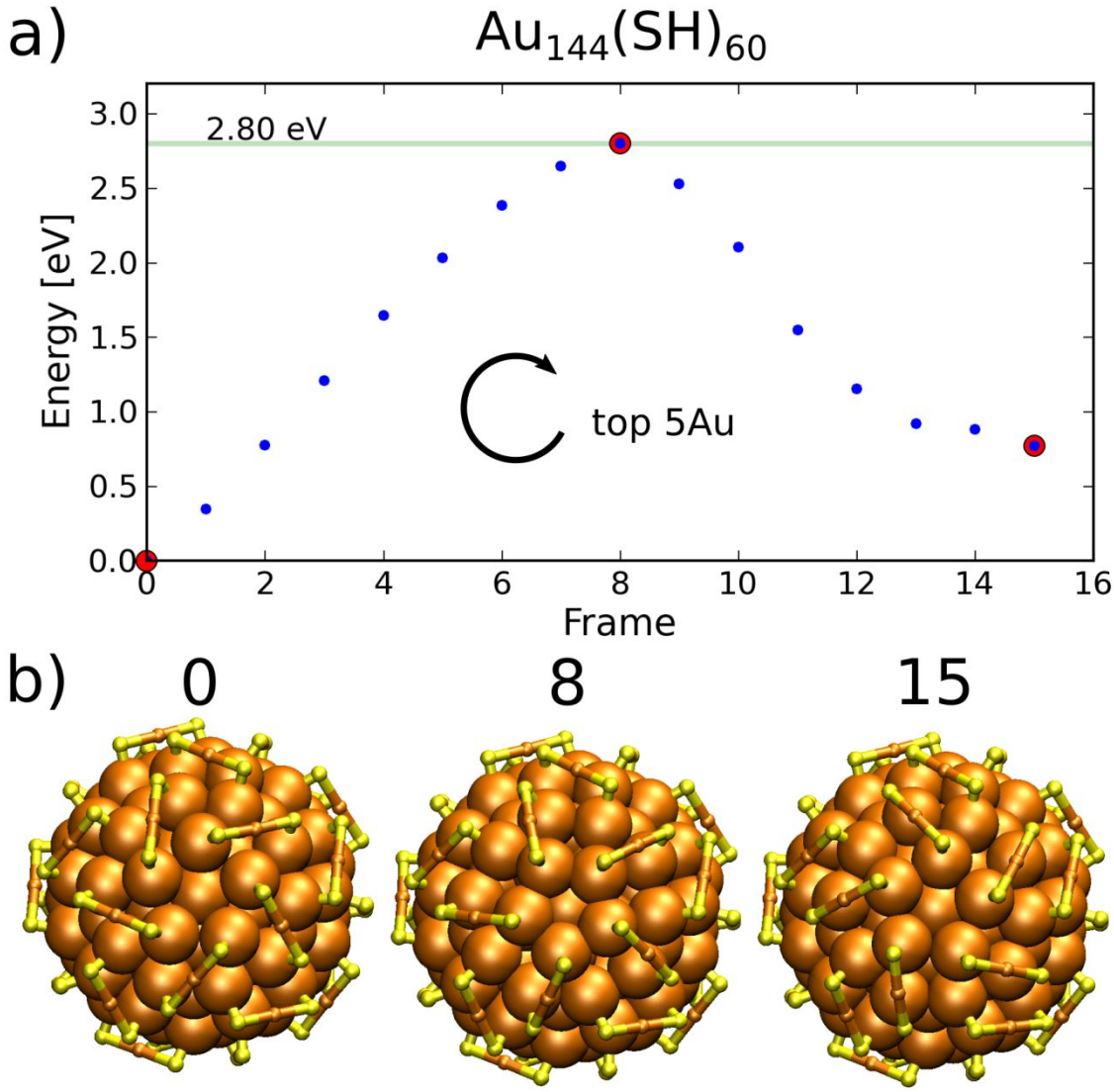

Figure 4. Inversion energy profile and selected configurations of $Au_{144}(SH)_{60}$ by rotation of the five core Au-atoms closest to the C5 symmetry axis parallel to the top view direction. Behavior of the energy as a function of reaction frame is given in (a) and selected frames are shown in (b) corresponding to red data points in (a). Only the gold-sulfur framework is shown for clarity. Arrow in (a) denotes the direction of the rotation.

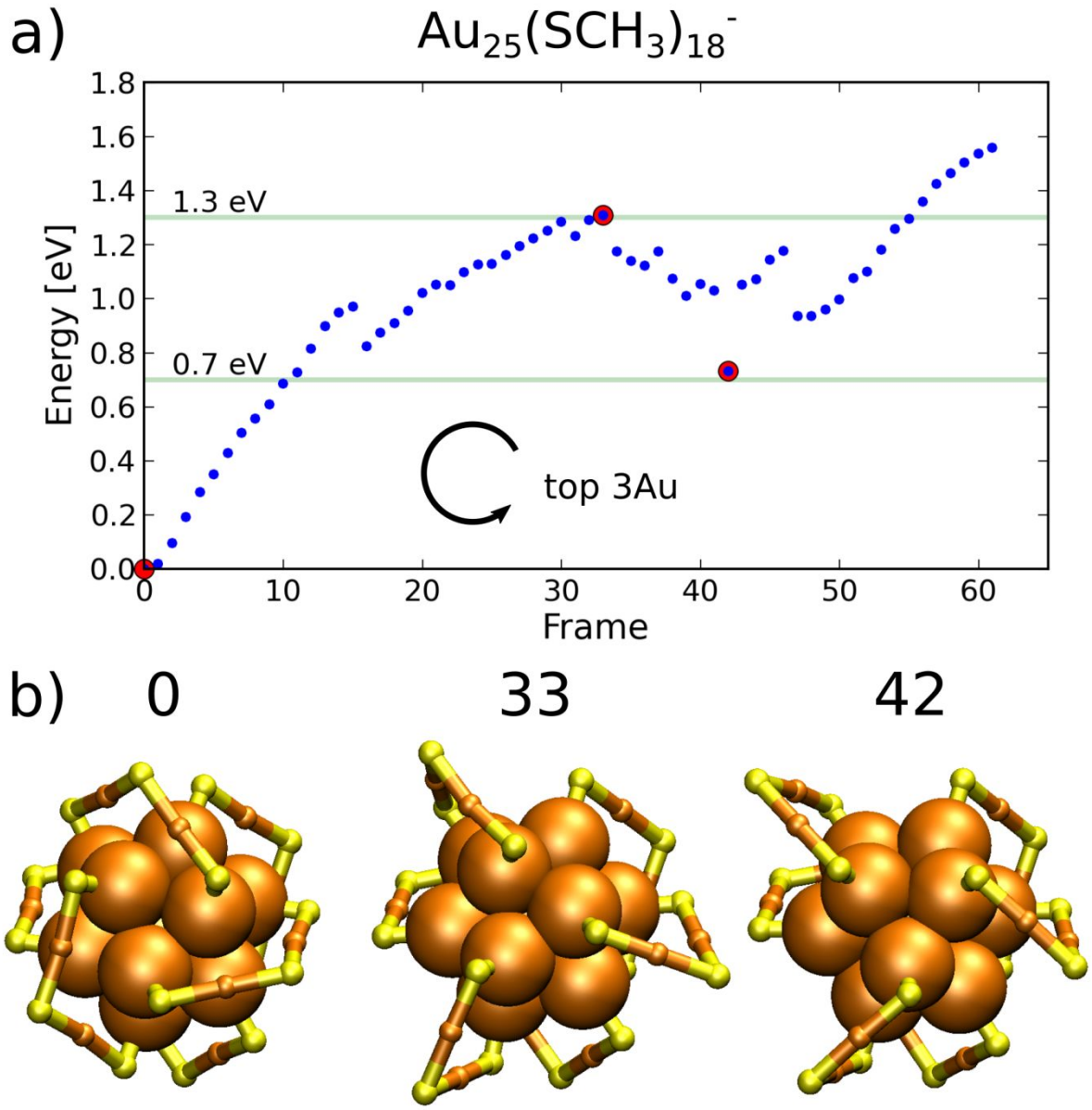

Figure 5. Transformation of $[Au_{25}(SCH_3)_{18}]^-$ by rotation of the three core Au-atoms closest to the C3 symmetry axis. The energy profile is given in (a) and selected structures in (b) corresponding to red data points in (a). Only the gold-sulfur framework is shown for clarity. Arrow in (a) denotes the direction of the rotation.

TOC graphics